



Article

Electrical Impedance Spectroscopy as a Tool to Detect the Epithelial to Mesenchymal Transition in Prostate Cancer Cells

Lexi L. C. Simpkins ^{1,2} , Luis A. Henriquez ^{1,2}, Mary Tran ^{1,2} and Tayloria N. G. Adams ^{1,2,3,4,*}

¹ Department of Chemical and Biomolecular Engineering, University of California Irvine, Irvine, CA 92697, USA; crowelll@uci.edu (L.L.C.S.); lhenriq1@uci.edu (L.A.H.); phuctt2@uci.edu (M.T.)

² Sue and Bill Gross Stem Cell Research Center, University of California Irvine, Irvine, CA 92697, USA

³ Department of Biomedical Engineering, University of California Irvine, Irvine, CA 92697, USA

⁴ Department of Materials and Science Engineering, University of California Irvine, Irvine, CA 92697, USA

* Correspondence: tayloria@uci.edu

Abstract: Prostate cancer (PCa) remains a significant health threat, with chemoresistance and recurrence posing major challenges despite advances in treatment. The epithelial to mesenchymal transition (EMT), a biochemical process where cells lose epithelial features and gain mesenchymal traits, is linked to chemoresistance and metastasis. Electrical impedance spectroscopy (EIS), a novel label-free electrokinetic technique, offers promise in detecting cell phenotype changes. In this study, we employed EIS to detect EMT in prostate cancer cells (PCCs). PC3, DU145, and LNCaP cells were treated with EMT induction media for five days. EIS characterization revealed unique impedance spectra correlating with metastatic potential, distinguishing DU145 EMT+ and EMT– cells, and LNCaP EMT+ and EMT– cells (in combination with dielectrophoresis), with comparisons made to epithelial and mesenchymal controls. These changes were supported by shifts in electrical signatures, morphologies, and protein expression, including the downregulation of E-cadherin and upregulation of vimentin. No phenotype change was observed in PC3 cells, which maintained a mesenchymal phenotype. EMT+ cells were also distinguishable from mixtures of EMT+ and EMT– cells. This study demonstrates key advancements: the application of EIS and dielectrophoresis for label-free EMT detection in PCCs, characterization of cell electrical signatures after EMT, and EIS sensitivity to EMT transitions. Detecting EMT in PCa is important to the development of more effective treatments and overcoming the challenges of chemoresistance.



Citation: Simpkins, L.L.C.; Henriquez, L.A.; Tran, M.; Adams, T.N.G.

Electrical Impedance Spectroscopy as a Tool to Detect the Epithelial to Mesenchymal Transition in Prostate Cancer Cells. *Biosensors* **2024**, *14*, 503.

<https://doi.org/10.3390/bios14100503>

Received: 30 July 2024

Revised: 7 October 2024

Accepted: 10 October 2024

Published: 15 October 2024



Copyright: © 2024 by the authors. Licensee MDPI, Basel, Switzerland. This article is an open access article distributed under the terms and conditions of the Creative Commons Attribution (CC BY) license (<https://creativecommons.org/licenses/by/4.0/>).

1. Introduction

In the United States, prostate cancer (PCa) poses a significant health threat and has the highest incidence of cancer amongst men, with an estimated 300,000 new cases and 35,000 deaths expected in 2024. Yet, significant gains have been made in survival rates, with a 50% decrease in deaths since the mid-1990s [1]. With advances in medicine, patients may undergo surgical, radiotherapy, and chemotherapy treatments to combat PCa [2]. However, even after radical prostatectomy, there remains a possibility for cancer recurrence [3], representing a progression in PCa that is challenging to treat. The probability of recurrence lies between 15 and 40% in a span of 10 years [3]. Recurrence may occur locally, or the cancer may metastasize, leading to death. Consequently, addressing recurrence in a clinical setting is crucial for improving long-term patient outcomes.

PCa metastasis remains a challenge not only due to the spread of cancer to distant organs but also due to subsequent tumor heterogeneity and plasticity [4]. These factors impact the effectiveness of PCa treatments. One hallmark of metastasis is the epithelial to mesenchymal transition (EMT), a reversible process in which polarized epithelial cells undergo biochemical changes, ultimately leading to transformation into mesenchymal

cells [5], which is distinguishable by increased chemoresistance [6]. During EMT, cells upregulate the expression of mesenchymal markers such as N-cadherin and vimentin, leading to aggressiveness and invasiveness, while downregulating epithelial markers such as E-cadherin and ZO-1, resulting in the loosening of cell junctions, the disruption of cell-to-cell contact, and the development of elongated, motile spindle-shaped cells with increased resistance to apoptosis [5,7]. Subsequent effects of EMT include cells' ability to self-renew and increases in the heterogeneity of the cell population [8]. Several cell signaling pathways induce EMT, including transforming growth factor beta (TGF- β), Wnt, notch, sonic hedgehog, and interleukin-6 [7]. Thus, cancer cells exist in two states: an epithelial state, characterized by high polarity, strong cell-to-cell adhesion, cobblestone morphology, and low chemoresistance, and a mesenchymal state, characterized by low polarity, reduced cell-to-cell adhesion, spindle-like elongated morphology, high migratory capabilities, and increased chemoresistance [7].

Despite extensive research and the recognized role of EMT in chemoresistance, no approved clinical application for EMT markers currently exists. Consequently, alternative methods such as electrical impedance spectroscopy (EIS) are worthy of exploration due to their ability to detect phenotypic changes in cells [9]. EIS is a non-invasive electrokinetic technique that leverages the inherent electrical properties of cells to distinguish various types of cancer cells [10] and assess their dynamic processes, including adhesion [11], proliferation [12], spreading [13], motility [14], and apoptosis [15], as well as chemoresistance [16]. Briefly, EIS uses nonuniform electric fields to interact with cell membranes, membrane proteins, and intracellular molecules [17]. The resulting impedance spectra have frequency-dependent characteristics unique to the cell population being examined. For a comprehensive review of EIS theory, refer to [16,18]. At radio frequencies, the impedance spectra provide valuable insight into biological cells including surface charge mobility, cell membrane thickness, and relaxation effects caused by proteins, amino acid residues, and internal organelles [17]. Thus, for prostate cancer cells (PCCs), selectively investigating radio frequency EIS responses can reveal intrinsic and extrinsic factors that contribute to the cell phenotype, such as those associated with EMT.

To the authors' knowledge, there are currently no studies using EIS to study EMT in PCCs. However, EIS has been used to distinguish PCC lines [9,19], and other impedimetric techniques such as electric cell-substrate impedance sensing (ECIS) [20] and impedance flow cytometry (IFC) [21] have been used to monitor EMT in lung and breast cancer cells. If we expand to include electrochemical immunosensors, then several studies have investigated EMT for liver, breast, ovarian, and pancreatic cancer cells [22,23]. While all of these impedimetric techniques are valuable for studying EMT in cancer cells, our specific focus remains on EIS.

In this study, the EIS of three PCC lines that underwent EMT induction were characterized. The PC3 cell line, derived from a vertebral metastasis lesion of grade IV prostatic adenocarcinoma in a 62-year-old male [24], and the DU145 cell line, from a 69-year-old male with lymphocytic leukemia and advanced prostate carcinoma [25], were analyzed alongside the androgen-dependent LNCaP cell line, which originated from a metastatic lesion of prostatic adenocarcinoma in a male [26]. PCCs were treated with EMT induction media over five days and characterized using EIS in a simple parallel-electrode microfluidic device and, in some cases, by dielectrophoresis, an alternative electrokinetic technique. Our results showed that PC3, DU145, and LNCaP cells have unique electrical signatures without and with EMT treatment (EMT– and EMT+). We verified EMT induction with several outputs: the discernible difference in the impedance spectra, comparison of the impedance spectra of PC3 and DU145 cells to epithelial (human primary prostate cells, HPrECs) and mesenchymal (human mesenchymal stem cells, hMSCs) controls, cell morphology assessment, and immunofluorescent imaging of E-cadherin and vimentin protein expression. Additionally, dielectrophoresis analysis distinguished the LNCaP EMT+ and EMT– cells. These outputs confirmed that the EMT was successfully induced in the DU145 and the LNCaP cells but not in the PC3 cells. These findings demonstrate the potential of

EIS to detect EMT-specific phenotype changes in PCCs and highlight several key advancements: the application of EIS and dielectrophoresis for label-free EMT detection in PCCs, characterization of changes in cell electrical signatures with EMT, and demonstration of the sensitivity of EIS to EMT transitions.

2. Materials and Methods

2.1. Cell Culture

PC3, DU145, and LNCaP cells were obtained from American Type Culture Collection (ATCC, Manassas, VA, USA). These cells were subcultured in Roswell Park Memorial Institute (RPMI)-1640 medium (Thermo Fisher, A1049101, Waltham, MA, USA) supplemented with 10% (*v/v*) heat-inactivated fetal bovine serum (Life Technologies, Carlsbad, CA, USA, 18121001), 50 U mL⁻¹ penicillin, and 50 µg mL⁻¹ streptomycin (Life Technologies, Carlsbad, CA, USA, 15140122) at 37 °C in a humidified 5% CO₂ incubator.

Umbilical cord-derived hMSCs obtained from ATCC (PCS-500-100) were subcultured in MSC basal medium (ATCC, PCS-500-030) supplemented with a growth kit, low serum (ATCC, PCS-500-040), at 37 °C in a humidified 5% CO₂ incubator. HPrECs were obtained from ATCC (PCS-440-010) and subcultured in prostate epithelial cell basal medium (ATCC, PCS-440-030) supplemented with a prostate epithelial cell growth kit (ATCC, PCS-440-040) at 37 °C in a humidified 5% CO₂ incubator.

2.2. EMT Treatment

PC3, DU145, and LNCaP cells were treated with StemXVivio EMT-induction media supplement (R&D Systems, Minneapolis, MN, USA, CM017) according to the manufacturer's instructions. Specifically, two days after seeding 30,000 cells, the growth media was replaced with growth media supplemented with 1% EMT-inducing media. The EMT media was refreshed after 48 h, and the cells were cultured in the EMT media for 5 days. On Day 6, the cells were processed for electrokinetic, morphology, and immunofluorescent analyses.

2.3. Cell Preparation for Electrokinetic Characterization

After EMT treatment, the monolayer of cells was rinsed once with 1X Dulbecco's phosphate-buffered saline (DPBS) (Life Technologies, Carlsbad, CA, USA) followed by trypsinization with 0.05% Trypsin-EDTA (Life Technologies, Carlsbad, CA, USA) for 5 min. Once cells were detached from the culture plate, they were neutralized with an equal volume of a growth medium. The cell suspension was centrifuged at 150 × g for 5 min to pellet the cells. A low-conductivity buffer (LCB) was made with Milli-Q water containing 8.5% (*w/v*) sucrose and 0.3% (*w/v*) D-glucose. The conductivity was adjusted to 100 ± 5 µS/cm using RPMI-1640 (Thermo Fisher, 11875135). The LCB was passed through a 22-micron filter for sterilization. Next, the cell pellet was washed three times in the LCB at 150 × g for 5 min. For the final resuspension, the cell concentration was adjusted to 300,000 cells/mL. The following samples were assessed: PC3 EMT-, PC3 EMT+, DU145 EMT-, DU145 EMT+, LNCaP EMT-, and LNCaP EMT+, as well as mixtures of PC3 EMT-/EMT+, DU145 EMT-/+ and LNCaP EMT-/+ cells.

2.4. Electrokinetic Characterization with EIS

For EIS, a simple microwell device with parallel electrodes was fabricated using previously published techniques [27,28] with electrode dimensions of a 50 µm width and 100 µm gap between the electrodes. The microfluidic device was washed 3 times with the LCB and attached to a Reference 600+ Potentiostat/Galvanostat/ZRA (Gamry Instruments, Warminster, PA, USA). The EIS characterization was completed using a frequency sweep from 350 Hz to 5 MHz at 10 mV for 5 min. At least 3 to 5 technical replicates were completed for each independent experiment. This characterization was repeated for three biological replicates (*n* = 3) of the PC3, DU145, and LNCaP cells. For hMSCs and HPrECs, the experiments were completed for three biological replicates (*n* = 3).

2.5. Analysis of EIS Data

Once the EIS data were collected, outliers were removed using Prism 10. With the outliers removed, the technical replicates were normalized to eliminate any dependence on the LCB. Normalization was performed by dividing the measured cell impedance at each frequency by the measured LCB impedance at the same frequency, given by

$$Z_{normalized} = \frac{Z_{C,f_i}}{Z_{LCB,f_i}} \quad (1)$$

where $Z_{normalized}$ is the normalized impedance, Z_{C,f_i} is the cell impedance at frequency f_i , Z_{LCB,f_i} is the buffer impedance at frequency f_i , and i represents each frequency in the sweep. The normalized impedance spectra for each of the biological replicates ($n = 3$) of the PC3, DU145, and LNCaP cells were averaged to plot an average impedance spectrum. This process was repeated for the hMSCs and HPrECs. Additionally, the averaged normalized impedance over the tested frequency range was calculated. A one-way ANOVA with Tukey's multiple comparisons was performed on the average impedance.

2.6. An Alternative Electrokinetic Characterization with Dielectrophoresis

For dielectrophoresis, a 3DEP analyzer (LabTech, East Sussex, Heathfield, UK) [29], an electrokinetic instrument similar to the potentiostat in the use of nonuniform electric fields to assess biological cells, was used to characterize the LNCaP cells. The 3DEP analyzer uses a microfluidic device with an array of 20 microwells containing 3-dimensional circular electrodes for cell measurements. Each microwell can supply an independent frequency with the same voltage. This microfluidic device was rinsed with 100 μ L of 70% ethanol (1 time), Milli-Q water (3 times), and the LCB (3 times). After, 80 μ L of the resuspended LNCaP cells were introduced into the microfluidic device with a 200 μ L pipet and the device was covered with an 18 mm \times 18 mm glass coverslip. The microfluidic device was placed inside the 3DEP analyzer and a frequency sweep from 10 kHz to 20 MHz at 10 Vpp was completed in 60 s. The 3DEP analyzer outputs a relative cell response based on variations in light intensity as a function of frequency [30]. The cell response was evaluated, and outliers removed with the 3DEP analyzer software version 3. This characterization was repeated for three biological replicates.

2.7. EMT Characterization with Morphology Assessment

After EMT treatment, the PC3, DU145, and LNCaP cells were rinsed with 1 \times DPBS then fixed with a 4% paraformaldehyde solution for 10 min. Cells were incubated in a Hoechst 33342 solution (Life Technologies, Carlsbad, CA, USA) at a 1:2500 dilution in 1 \times DPBS for 5 min to visualize the nuclei and then rinsed twice with 1 \times DPBS. The Keyence BZ-X800 All-in-one Fluorescence Microscope (Keyence, Itasca, IL, USA) was used for imaging.

2.8. EMT Characterization with Immunofluorescence

After EMT treatment, cells were rinsed with 1 \times DPBS and then fixed with a 4% paraformaldehyde solution for 10 min. Cells were rinsed in 1 \times DPBS and then permeabilized in 0.2% Triton X for 30 min. The cells were washed with 1 \times DPBS and then incubated in a blocking buffer consisting of 5% (v/v) normal donkey serum (Jackson ImmunoResearch, West Grove, PA, USA) and 1% (w/v) bovine serum albumin (Life Technologies, Carlsbad, CA, USA) for 15 min. This was followed by incubation in primary antibodies for 1 h at room temperature, a rabbit E-cadherin polyclonal antibody (Invitrogen, Waltham, MA, USA, 1:100 dilution), mouse ZO-1 monoclonal antibody (Invitrogen, Waltham, MA, USA, clone A12, 1:100 dilution), rabbit N-cadherin polyclonal antibody (Invitrogen, Waltham, MA, USA, at a 1:100 dilution), and rabbit vimentin polyclonal antibody (Invitrogen, Waltham, MA, USA, 1:100 dilution), were all diluted in the blocking buffer. Cells were subsequently washed with 1 \times DPBS and then incubated with secondary antibodies: donkey anti-rabbit AlexaFluor488 (Life Technologies, Carlsbad, CA, USA)

and donkey anti-mouse AlexFluor594 (Life Technologies, Carlsbad, CA, USA) diluted in a 1% blocking buffer for 4 h at room temperature. Afterwards, cells were incubated in a Hoechst 33342 Solution (Life Technologies, Carlsbad, CA, USA, 1:2500 dilution in 1× DPBS) for 5 min to visualize the nuclei and then rinsed twice with 1× DPBS. The Keyence BZ-X800 All-in-one Fluorescence Microscope was used for imaging.

After imaging, the green channel intensity from the immunofluorescent images was quantified using ImageJ version 1.80. Each image was imported and split into its red, green, and blue (RGB) channels. Only the green channel, corresponding to the fluorescent signal, was analyzed. The red and blue channels were discarded. To ensure consistent measurements across images, a rectangular region of interest (ROI) was defined using the rectangle tool and placed in the same location for each image. Two ROIs per image were used to assess different areas of the image and obtain an average fluorescence intensity. The average green channel intensity for each marker (E-cadherin and vimentin) was calculated and plotted to compare fluorescence levels. A one-way ANOVA with Šidák's multiple comparisons was performed on the average intensity.

3. Results

The EMT was induced in PCCs and characterized using EIS (or dielectrophoresis), morphology assessments, and immunofluorescent staining; Figure 1 depicts the EMT and outlines the experimental workflow. During EMT, cells lose epithelial features, noted by the downregulation of epithelial markers such as E-cadherin and ZO-1, and gain mesenchymal features noted by the upregulation of mesenchymal markers such as N-cadherin and vimentin. An intermediate phenotype, where both epithelial and mesenchymal markers are present, can also occur, Figure 1 (1). To initiate the EMT, PC3, DU145, and LNCaP cells were treated for 5 days with EMT-inducing media, Figure 1 (2). After the EMT treatment, the cells were characterized using EIS (or dielectrophoresis) and the phenotype change was visually confirmed by nuclei stain and immunofluorescence imaging, Figure 1 (3). Supplemental Figure S1 illustrates the method used to quantify the intensity of the fluorescent stains. Prism 10 was used to analyze the impedance spectra; the technical replicates were analyzed for outliers, normalized, and averaged.

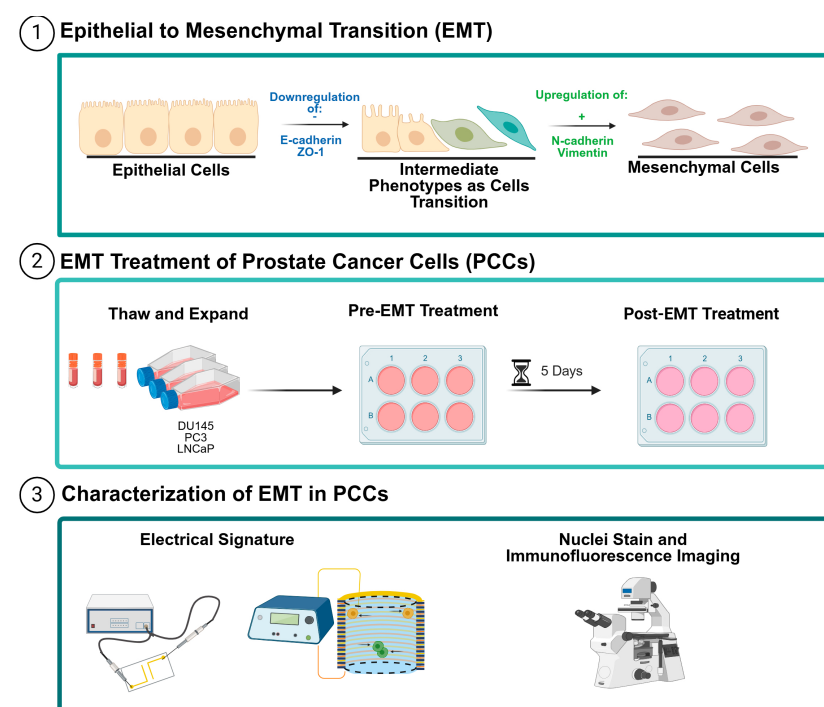


Figure 1. The EIS experimental workflow for characterizing phenotype changes in PCCs. (1) An illustration of EMT in cancer cells. Initially, cells exhibit an epithelial phenotype characterized by the

expression of E-cadherin and ZO-1. Then, the cells undergo the downregulation of E-cadherin and ZO-1, transitioning to an intermediate phenotype. In this stage, there is a shift in the protein expression profile with an upregulation of N-cadherin and vimentin, leading to the mesenchymal phenotype. (2) DU145, PC3, and LNCaP cells were obtained from cryogenic storage, thawed, and expanded in proliferation media. Cells were seeded with EMT-inducing media and allowed 5 days to incubate. (3) Cells were characterized using EIS and the 3DEP analyzer. A phenotype change was validated by a nuclei stain and immunofluorescence imaging. The figure was created with Biorender.com.

3.1. Electrical Signature of PCCs

The impedance spectra of PCCs were collected, normalized to remove dependency on LCB, and averaged. Figure 2 shows the unnormalized and normalized Bode plot over the frequency range 350 Hz–5 MHz of one passage ($n = 1$ biological replicate) of PC3 EMT+ and DU145 EMT+ cells. For both PC3 and DU145 cells, the impedance decreases with increased frequency, displaying the typical s-shape impedance spectrum. Comparing Figure 2A,C, the impedance spectra of the PC3 and DU145 cells are defined by two transitions (10^2 – 10^3 Hz and 10^6 – 10^7 Hz) and a plateau (10^3 – 10^6 Hz). This trend remains when comparing the normalized plots, Figure 2B,D. The technical replicates for the PC3 cells have a smaller spread than DU145 cells.

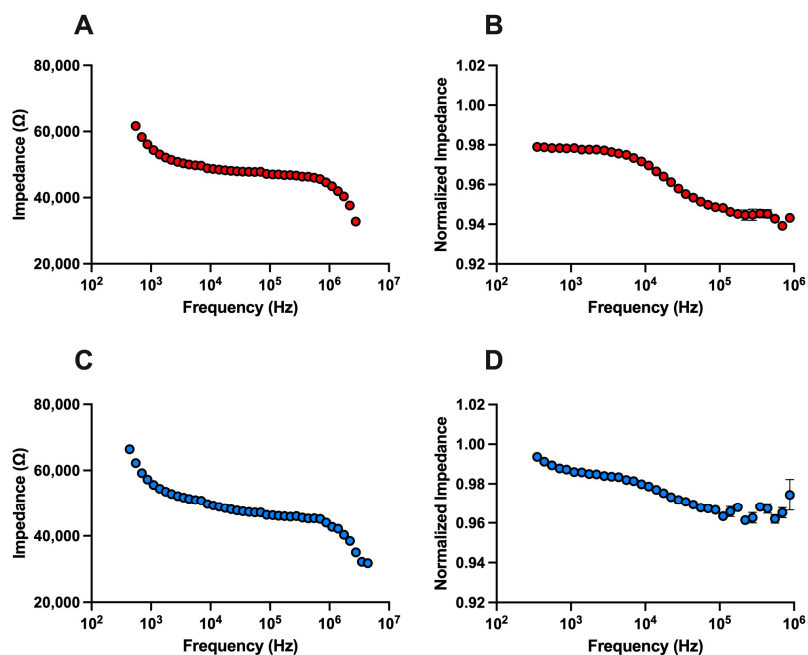


Figure 2. EIS cell analysis of PCCs. (A) Unnormalized and (B) normalized EIS spectrum of PC3 EMT+ cells ($n = 1$). (C) Unnormalized and (D) normalized EIS spectrum of DU145 EMT+ cells ($n = 1$). In all plots, data points represent average impedance, technical replicates equal 3 to 5 individual measurements, and error bars are standard error mean. Most error bars in (A–D) are too small to be visualized.

We completed the EMT treatment and measured the impedance signature of PC3 and DU145 cells. Figure 3A,B presents the normalized impedance of three biological replicates ($n = 3$) of the PC3 and DU145 cells, respectively. EMT+ signifies that cells were treated with EMT induction media and EMT– signifies that cells were not treated. Similar to Figure 2, the impedance decreased with increased frequency. There is a small separation in the impedance spectra for the PC3 EMT+ and PC3 EMT– cells with the error bars overlapping. In contrast, there is a noticeable separation in the impedance spectra for the

DU145 EMT+ and DU145 EMT– cells and the error bars do not overlap. Figure 3C,D shows the impedance spectra of PC3 and DU145 cells compared to the epithelial (HPrECs) and mesenchymal (hMSCs) controls. HPrECs serve as the negative control for EMT induction while hMSCs serve as the positive control for EMT induction. The impedance spectrum of the mesenchymal control is higher than that of the epithelial control. The averaged impedance spectrum of DU145 EMT– cells falls below and overlaps the epithelial control. The DU145 EMT+ cells initially overlap with the epithelial control but shift upward with increasing frequency, moving closer to the mesenchymal control. The error bars of the DU145 EMT– cells overlap with the error bars of the epithelial control. In contrast, the average impedance spectra of PC3 EMT– cells and PC3 EMT+ cells overlap the mesenchymal control. The error bars of the PC3 EMT– cells and PC3 EMT+ cells overlap with each other and the mesenchymal control. In Figure 3E,F, the averaged normalized impedance of PC3 EMT– and PC3 EMT+ cells are similar, while the average normalized impedance of DU145 EMT– and DU145 EMT+ cells differ with statistical significance ($** p < 0.05$). Also, the average normalized impedance for the epithelial and mesenchymal control are different with statistical significance. Each DU145 condition (EMT– and EMT+) differs significantly from both the epithelial and mesenchymal controls.

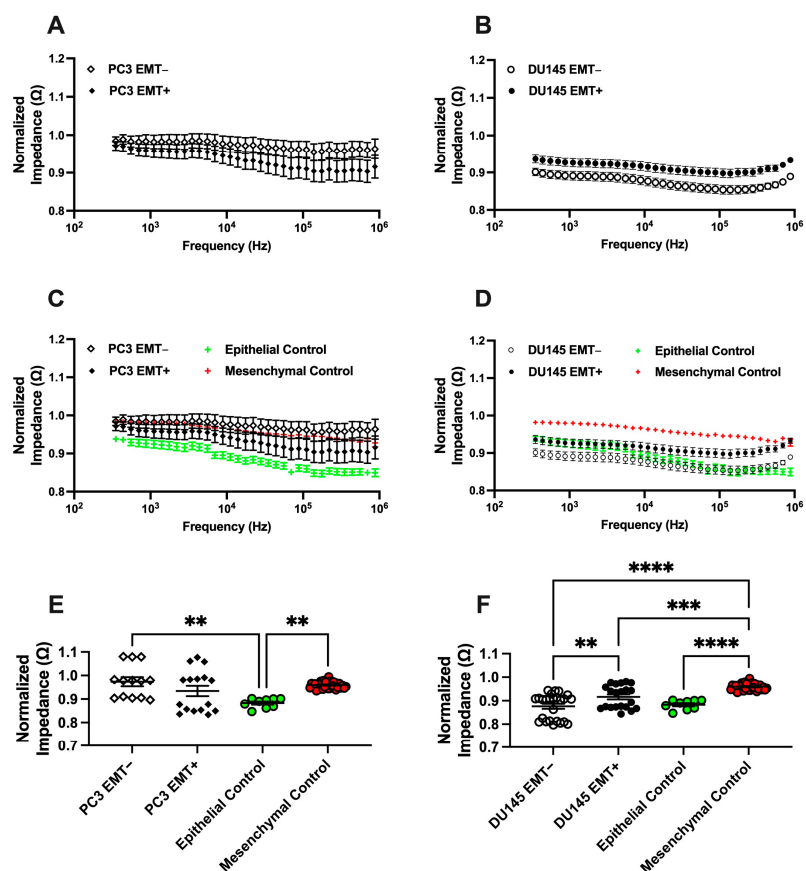


Figure 3. Normalized EIS cell analysis of EMT-treated PCCs. (A) Average spectra of PC3 EMT– cells and PC3 EMT+ cells. (B) Average spectra of DU145 EMT– cells and DU145 EMT+ cells. Average spectra of (C) PC3 EMT– and PC3 EMT+ cells and (D) DU145 EMT– and DU145 EMT+ cells compared to epithelial and mesenchymal controls. Average normalized impedance of (E) PC3 EMT– and PC3+ cells and (F) DU145 EMT– and DU145 EMT+ cells compared to epithelial and mesenchymal controls. Error bars represent standard error mean. $n = 3$ for PC3, DU145, epithelial control, and mesenchymal control cells. Statistical analysis completed on pooled data sets; $** p < 0.05$, $*** p < 0.001$, and $**** p < 0.0001$.

The electrical signature of LNCaP cells treated with EMT induction media was determined with EIS and the 3DEP analyzer. Small differences at select frequencies were observed for both the impedance and DEP spectra. At higher frequencies, the impedance spectra shows that LNCaP EMT⁻ cells have higher impedance than LNCaP EMT⁺ cells, with overlap occurring at lower frequencies, Supplemental Figure S2. In the DEP spectra, LNCaP EMT⁻ cells exhibit higher light intensity response at certain frequencies, while at lower frequencies, LNCaP EMT⁺ cells show a greater response, Supplemental Figure S3.

To further analyze the ability of EIS to detect EMT, impedance signal ratios were calculated for PC3, DU145, and LNCaP cells and are presented in Supplemental Table S1, with guidance on interpretation provided in Supplemental Table S2. Deviations or lack of deviations from a ratio of one are used to assess changes in cell state. The EMT⁻ cell/EMT⁺ cell ratio and the EMT⁺ cell/mesenchymal control ratio deviate from one for the DU145 and LNCaP cells. However, the EMT⁻ cell/EMT⁺ cell ratio for PC3 remains close to one. The epithelial control/mesenchymal control ratio acts as a baseline for the impedance signal, offering context for comparison across cell lines.

Additional EIS measurements were performed on mixtures of PC3 EMT^{-/+}, DU145 EMT^{-/+}, and LNCaP EMT^{-/+} cells. Supplemental Figure S4 shows that differences in the impedance spectra are observed at higher frequencies for DU145 EMT⁻, DU145 EMT⁺, and DU145 EMT^{-/+} cells, as well as for LNCaP EMT⁻, LNCaP EMT⁺, and LNCaP EMT^{-/+} cells. At lower frequencies, there is overlap among the three conditions for both DU145 and LNCaP cells. For PC3 cells, the impedance spectra of EMT^{-/+} mixtures align closely with those of EMT⁻ cells.

3.2. Biological Assessment of EMT Treatment

It is necessary to characterize the EMT using biological markers. Thus, we examined the morphology and protein expression of the PCCs after EMT treatment. Figure 4 presents nuclei stains of PC3, DU145, and LNCaP cells. The PC3 EMT⁻ and EMT⁺ cells do not exhibit any differences in their morphology; they are spindle-like and fibroblastic. For the DU145 cells, the EMT⁻ cells have a cobblestone morphology while EMT⁺ cells feature a spindle-like, fibroblastic morphology. The LNCaP EMT⁻ cells show a similar cobblestone morphology, while the LNCaP EMT⁺ cells show a more fibroblastic morphology.

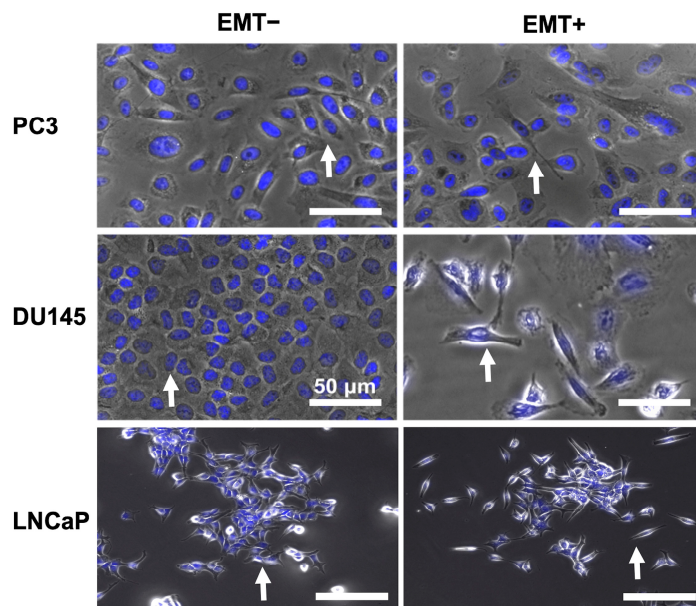


Figure 4. Morphology assessment of EMT-treated PCCs. Phase contrast images overlaid with Hoechst-stained nuclei of PC3, DU145, and LNCaP cells without (EMT⁻) and with EMT (EMT⁺) treatment. The white arrows indicate a representative cell exhibiting characteristic epithelial morphology under EMT⁻ conditions and mesenchymal morphology under EMT⁺ conditions.

Figure 5 displays the protein expression of E-cadherin and vimentin for the PCCs with immunofluorescence staining and fluorescent intensity quantification. For the PC3 cells, a decrease in fluorescence is observed and quantified for both E-cadherin and vimentin. The DU145 cells show positive fluorescence for E-cadherin and vimentin; however, the E-cadherin expression decreased following EMT treatment, while vimentin expression increased. Similarly, LNCaP cells exhibited positive fluorescence for E-cadherin and vimentin, with a decrease in E-cadherin after EMT treatment and increased vimentin expression. To complement the fluorescent intensity analysis, a ‘true/false’ classification was used to assess the protein staining results, Supplemental Table S3. ZO-1 was used as an additional epithelial marker, and downregulation was observed in DU145 EMT+ cells, Supplemental Figure S5. N-cadherin was used as an additional mesenchymal marker, and upregulation was observed in LNCaP EMT+ cells, Supplemental Figure S6.

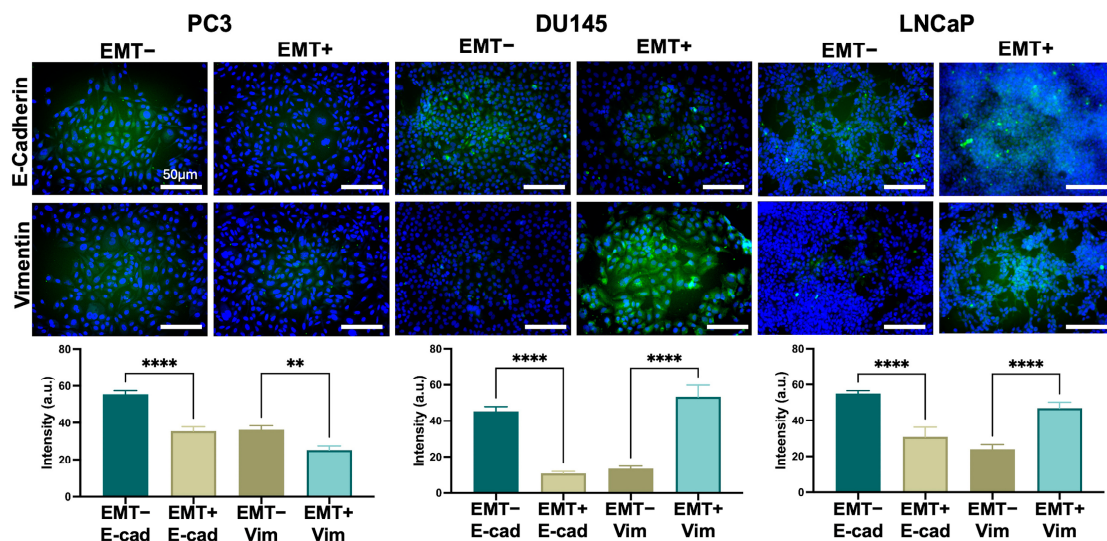


Figure 5. Immunofluorescent staining of PCCs without and with EMT treatment (EMT– and EMT+, respectively). The staining highlights the expression of epithelial marker E-cadherin and mesenchymal marker vimentin, both tagged with fluorescent labels. The quantification of fluorescent intensity for each marker is provided in the bar charts. Error bars represent the standard error mean. $n = 3$ for all conditions. The statistical analysis was completed on pooled data sets; ** $p < 0.05$, and **** $p < 0.0001$.

4. Discussion

Characterizing the electrical signature of phenotype changes, such as the EMT, in PCCs is essential as it correlates with chemoresistance [6]. The EMT involves the transition of cells through multiple states marked by morphological, protein, gene, and electrical changes in their phenotype. EIS effectively analyzes cell phenotypes by measuring impedance induced by internal and external factors. To capture changes in the electrical signature associated with EMT, we examined frequencies from 350 Hz to 5 MHz. This range detects changes in the cell membrane properties potentially related to the loosening of tight junctions and changes in membrane structure. We chose PC3, DU145, and LNCaP cell lines based on their varying metastatic potentials [25,31,32] and levels of cancer stem-like cells [33]. Also, these cells are frequently used in PCa research [34], making them suitable for this study. Thus, the focus was on inducing the EMT in PC3, DU145, and LNCaP cells and detecting a phenotype change with EIS or dielectrophoresis. The novelty lies in the label-free engineering measurement of cells’ electrical signature combined with morphology and immunofluorescent assessments to detect PCC phenotype changes related to EMT.

In this study, we treated PCCs with EMT induction media and identified cell phenotype changes using EIS. Our results show that the impedance of PC3 EMT+ cells is higher than the DU145 EMT+ cells. Similarly, we observed that the impedance of PC3 EMT– cells is

higher than the DU145 EMT– cells. These findings represent Day 5 EIS measurements. In contrast, our previous study, which included Day 1 and Day 7 EIS measurements with no EMT treatment, showed that the impedance of DU145 cells was higher than PC3 cells on Day 1 [9], a finding also supported by study [19]. By Day 7, the impedance spectra indicated a higher impedance for PC3 cells compared to DU145 cells [9]. This shift aligns with our current findings and underscores the impact of cell culture duration on EIS measurements, confirming the consistency of impedance trends across studies. Additionally, it should be noted that EIS is sensitive enough to detect subtle day-to-day changes in cells.

EIS distinguished EMT+ and EMT– cells for the DU145 cells (Figure 3B,D,F), indicating a phenotype change. Similarly, the electrical signature of LNCaP cells, determined with EIS and dielectrophoresis, distinguished EMT+ and EMT– cells (Supplemental Figures S2 and S3). However, the EIS of EMT+ and EMT– cells for PC3 cells did not indicate a phenotype change. Additional comparisons to epithelial and mesenchymal controls provided more evidence of a phenotype change in the DU145 cells. Impedance signal ratios provide another view of EMT detection, with ratios that deviate from one suggesting a phenotype difference (Supplemental Tables S1 and S2). For DU145 and LNCaP cells, the EMT– cell to EMT+ cell ratio and the EMT+ to mesenchymal control ratio both deviated from one to a greater extent than in PC3 cells, supporting that these cells underwent a phenotype change, while PC3 cells did not. The epithelial control to mesenchymal control ratio provides a baseline for interpreting the impedance signal. Supplemental Figure S4 provides additional evidence of EIS distinguishing EMT+ and EMT– cells through the analysis of mixtures of DU145 and LNCaP cells.

As seen in Figure 4, there are morphological differences between the DU145 EMT– cells and the LNCaP EMT– cells featuring cobblestone morphology while DU145 EMT+ cells and LNCaP EMT+ cells display spindle-like, fibroblastic morphology. These alterations in morphology were due to the downregulation of E-cadherin in both DU145 and LNCaP cells (Figure 5), as supported by the complementary protein expression analysis (Supplemental Table S3), ZO-1 in DU145 cells (Supplemental Figure S5), and the upregulation in N-cadherin in LNCaP cells (Supplement Figure S6). Thus, we successfully induced and detected the occurrence of EMT in DU145 and LNCaP cells, distinguishing between epithelial state cells (EMT–) and mesenchymal state cells (EMT+). There was no phenotype change induced in PC3 cells because they were already in a mesenchymal state.

To our knowledge, this is the first study to utilize EIS to detect EMT in PCCs, demonstrating selectivity in distinguishing between epithelial (EMT–), mesenchymal (EMT+), and mixture (EMT–/+) phenotypes in DU145 and LNCaP cells. These results align with the hallmark impedimetric literature concerning phenotype changes during stem cell maturation [35–37]. An EMT detection procedure is described in the Supplemental Information, where we provide guidance on synthesizing the results of both early indicators (impedance assays using EIS) and later indicators (phenotypic assays, including morphology analysis and protein expression) of phenotype changes. This approach enables a robust assessment of whether cells have undergone EMT.

The application of impedimetric techniques to study EMT, as demonstrated in our study, is further supported by previous research showing the utility of these techniques in discerning EMT in various cancer models [20,21], underscoring the importance of electrical signatures in understanding cellular phenotypic plasticity. Specifically, Schneider et al. [20] treated lung (A549) and breast (MDA-MB231) cancer cells with TGF- β to induce EMT and characterized phenotype changes with morphology assessment, F-actin and ZO-1 protein expression, and an ECIS device with an array of circular electrodes. The A549 cells exhibited a shift from a cobblestone to a fibroblastic morphology, increased F-actin fibers, and decreased ZO-1 protein expression upon TGF- β treatment. ECIS enabled real-time, time-resolved impedance measurements of the adherent cells' dynamic responses to TGF- β , confirming the induction of EMT in A549 cells, while no changes were noted in the more aggressive MDA-MB231 line. Similarly, Zhao et al. [21] used IFC to detect EMT in A549 cells induced with TGF- β , discerning differences between A549 and A549 EMT based on

membrane capacitance and cytoplasm conductivity. The impedance differences observed by Zhao et al. were validated through microscopy, providing an analysis of EMT-induced changes in electrical properties.

Our work extends these investigations by applying EIS and dielectrophoresis to PCCs, offering a steady-state analysis of EMT-specific electrical changes. While Schneider et al. focused on the dynamic, real-time impedance changes, our approach provides a complementary perspective by evaluating steady-state electrical signatures of EMT– and EMT+ states in PCCs. Additionally, the use of a parallel-electrode microfluidic device in our study allows for a label-free analysis, reducing the need for antibody labeling, streamlining sample preparation and maintaining cell integrity. This contrasts with Zhao et al.'s single-cell IFC measurements, as our EIS and dielectrophoresis measurements provide an alternative platform for identifying EMT in bulk PCC populations without the need for fluid flow.

Furthermore, our study confirmed the induction of EMT in PCCs through typical morphology changes—a shift from a cobblestone to spindle-like phenotype—as well as through protein expression markers, including the downregulation of E-cadherin and upregulation of vimentin. These phenotypic shifts align with typical EMT-associated changes reported in other cancer models [22,38,39], underscoring the relevance of our findings. By comparing our steady-state EIS data to the dynamic and single-cell measurements of Schneider et al. and Zhao et al., our work broadens the scope of electrokinetic techniques to study EMT across different cancer types.

In the context of these previous studies, our research reinforces the utility of EIS in distinguishing between EMT+ and EMT– phenotypes in cancer cells, contributing to a rapidly growing body of literature on the application of label-free technologies in oncological research. Despite the advancements demonstrated by impedimetric techniques in characterizing EMT, challenges such as standardizing measurement protocols and interpreting complex impedance spectra persist. Our study's limitations, including variability in cell line responses and the need for larger sample sizes (such as fresh patient samples), emphasize the importance of addressing these constraints to fully leverage impedance spectroscopy in elucidating the dynamics of EMT and its implications for chemoresistance and cancer recurrence in PCa. Translating these insights into a clinical setting may require additional improvements in the EIS technology we use to ensure adequate sample preparation and developing cancer cell monitoring devices. However, there is value in the simplicity of our simple parallel-electrode device.

Despite these limitations, our findings have clinical relevance. EIS can be utilized to monitor and detect cancer cell dynamics in real time. Information from these studies can aid in the investigation of the molecular dynamics of EMT and provide more insight to when in time this program occurs in cancer cells. Characterizing the electrical signature of EMT can aid in creating drugs that target cancer cells susceptible to EMT; this strategy is underway for other cancers [7]. EIS can also be employed for drug development by assessing how effectively drugs target cancer cells undergoing EMT. This approach aligns with pharmaceutical industries' interest in developing drugs targeting specific cancer cell phenotypes. EIS extends to various clinical applications, including assessing EMT-associated metastatic potential through cell detachment and facilitating liquid biopsies. Coupling EIS with techniques like dielectrophoresis enables label-free processing and monitoring of cancer cells in patient samples, offering new insights into phenotypic characterization such as the visualization of heterogeneity.

5. Conclusions

EIS represents a promising tool for detecting and monitoring EMT in PCCs. This study presents important advancements, including the application of electrokinetic techniques (EIS and dielectrophoresis) for label-free EMT detection, characterization of electrical signatures of PCCs following EMT, and demonstration of sensitivity of these approaches to cellular transitions. Integrating impedimetric assays with traditional cancer diagnostic methods may enhance the early detection of cancer recurrence and enable timely, EMT-

targeted interventions, which are crucial for the long-term care of PCa patients. Future investigations will focus on employing label-free microfluidic cell sorting strategies to selectively isolate EMT-sensitive cells for further characterization. This will include an advanced electrokinetic analysis (generation of impedance and dielectrophoresis spectra), comprehensive molecular profiling to assess a wider range of epithelial and mesenchymal markers through protein and gene expression analyses, and imaging techniques (scanning electron microscopy). The advanced electrokinetic analysis will include microfluidic devices with single-cell and bulk-cell modalities, increased throughput, and increased sensitivity of the sensing electrodes to better identify EMT in PCCs.

Supplementary Materials: The following supporting information can be downloaded at: <https://www.mdpi.com/article/10.3390/bios14100503/s1>, Figure S1: Workflow for quantifying fluorescence intensity of immunofluorescent stains; Figure S2: EIS analysis of EMT-treated LNCaP cells. (A) Unnormalized and (B) normalized EIS spectrum of LNCaP EMT+ cells ($n = 1$). (C) Average spectra of LNCaP EMT– cells and LNCaP EMT+ cells; Figure S3: 3DEP analysis of EMT-treated LNCaP cells. (A) Average light intensity response spectra of LNCaP EMT– and EMT+ cells. (B) Black boxes highlight specific frequencies that emphasize differences in electrical signature between EMT– and EMT+ conditions; Table S1: Impedance signal ratio analysis of EMT-treated PCCs; Table S2: Interpretation of impedance signal ratios for EMT; Figure S4: EIS analysis of mixtures of EMT– and EMT+ cells. (A) Impedance spectra of average buffer. Normalized impedance spectra of mixtures for (B) PC3 ($n = 1$), DU145 ($n = 2$), and LNCaP ($n = 2$) cells; Table S3: The image classification of EMT status for cells. A “true” classification requires a ✓ mark in the EMT– E-cadherin box and a ✓ mark in the EMT+ Vimentin box. A “false” classification includes all other combinations. A ✓ mark indicates that most cells in the image are positive for the protein, and a ✗ indicates that most cells in the image are negative for the protein; Figure S5: Immunofluorescent staining of DU145 cells without and with EMT treatment (EMT– and EMT+, respectively). The staining highlights the protein expression of the epithelial marker ZO-1; Figure S6: Immunofluorescent staining of LNCaP cells without and with EMT treatment (EMT– and EMT+, respectively). The staining highlights the protein expression of the mesenchymal marker N-cadherin.

Author Contributions: Conceptualization, L.L.C.S., L.A.H., M.T. and T.N.G.A.; methodology, L.L.C.S., L.A.H., M.T. and T.N.G.A.; formal analysis, L.L.C.S., L.A.H. and M.T.; investigation, L.L.C.S., L.A.H. and M.T.; resources, T.N.G.A.; data curation, L.L.C.S., L.A.H. and M.T.; writing—original draft preparation, L.L.C.S., L.A.H., M.T. and T.N.G.A.; writing—review and editing, L.L.C.S., L.A.H., M.T. and T.N.G.A.; supervision, T.N.G.A.; funding acquisition, T.N.G.A. All authors have read and agreed to the published version of the manuscript.

Funding: This research was funded by the University of California Office of the President Cancer Research Coordinating Committee, grant number C22CR4143.

Institutional Review Board Statement: Not applicable.

Informed Consent Statement: Not applicable.

Data Availability Statement: Data are contained within the article.

Acknowledgments: The authors would like to thank UCI’s Integrated Nanosystems Research Facility for support with microfluidic device fabrication.

Conflicts of Interest: The authors declare no conflicts of interest.

References

1. Siegel, R.L.; Giaquinto, A.N.; Jemal, A. Cancer statistics, 2024. *CA A Cancer J. Clin.* **2024**, *74*, 12–49. [[CrossRef](#)]
2. Trewhatha, D.; Carter, K. Advances in prostate cancer treatment. *Nat. Rev. Drug Discov.* **2013**, *12*, 823. [[CrossRef](#)]
3. Wei, J.; Wu, X.; Li, Y.; Tao, X.; Wang, B.; Yin, G. Identification of Potential Predictor of Biochemical Recurrence in Prostate Cancer. *Int. J. Gen. Med.* **2022**, *15*, 4897–4905. [[CrossRef](#)]
4. Papanikolaou, S.; Vourda, A.; Syggelos, S.; Gyftopoulos, K. Cell Plasticity and Prostate Cancer: The Role of Epithelial–Mesenchymal Transition in Tumor Progression, Invasion, Metastasis and Cancer Therapy Resistance. *Cancers* **2021**, *13*, 2795. [[CrossRef](#)]
5. Kalluri, R.; Weinberg, R.A. The basics of epithelial-mesenchymal transition. *J. Clin. Investigig.* **2009**, *119*, 1420–1428. [[CrossRef](#)]

6. Wang, W.; Wang, L.; Mizokami, A.; Shi, J.; Zou, C.; Dai, J.; Keller, E.T.; Lu, Y.; Zhang, J. Down-regulation of E-cadherin enhances prostate cancer chemoresistance via Notch signaling. *Chin. J. Cancer* **2017**, *36*, 35. [[CrossRef](#)]
7. Du, B.; Shim, J.S. Targeting Epithelial–Mesenchymal Transition (EMT) to Overcome Drug Resistance in Cancer. *Molecules* **2016**, *21*, 965. [[CrossRef](#)]
8. Das, V.; Bhattacharya, S.; Chikkaputtaiah, C.; Hazra, S.; Pal, M. The basics of epithelial–mesenchymal transition (EMT): A study from a structure, dynamics, and functional perspective. *J. Cell. Physiol.* **2019**, *234*, 14535–14555. [[CrossRef](#)]
9. Crowell, L.L.; Yakisich, J.S.; Aufderheide, B.; Adams, T.N.G. Phenotypic Characterization of 2D and 3D Prostate Cancer Cell Systems Using Electrical Impedance Spectroscopy. *Biosensors* **2023**, *13*, 1036. [[CrossRef](#)] [[PubMed](#)]
10. Hong, J.-L.; Lan, K.-C.; Jang, L.-S. Electrical characteristics analysis of various cancer cells using a microfluidic device based on single-cell impedance measurement. *Sens. Actuators B Chem.* **2012**, *173*, 927–934. [[CrossRef](#)]
11. Qiu, Y.; Liao, R.; Zhang, X. Real-Time Monitoring Primary Cardiomyocyte Adhesion Based on Electrochemical Impedance Spectroscopy and Electrical Cell–Substrate Impedance Sensing. *Anal. Chem.* **2008**, *80*, 990–996. [[CrossRef](#)]
12. Daza, P.; Olmo, A.; Cañete, D.; Yúfera, A. Monitoring living cell assays with bio-impedance sensors. *Sens. Actuators B Chem.* **2013**, *176*, 605–610. [[CrossRef](#)]
13. Anh-Nguyen, T.; Tiberius, B.; Pliquett, U.; Urban, G.A. An impedance biosensor for monitoring cancer cell attachment, spreading and drug-induced apoptosis. *Sens. Actuators A Phys.* **2016**, *241*, 231–237. [[CrossRef](#)]
14. Giaever, I.; Keese, C.R. Micromotion of mammalian cells measured electrically. *Proc. Natl. Acad. Sci. USA* **1991**, *88*, 7896–7900. [[CrossRef](#)]
15. De Ninno, A.; Reale, R.; Giovinazzo, A.; Bertani, F.R.; Businaro, L.; Bisegna, P.; Matteucci, C.; Caselli, F. High-throughput label-free characterization of viable, necrotic and apoptotic human lymphoma cells in a coplanar-electrode microfluidic impedance chip. *Biosens. Bioelectron.* **2020**, *150*, 111887. [[CrossRef](#)]
16. Crowell, L.L.; Yakisich, J.S.; Aufderheide, B.; Adams, T.N. Electrical impedance spectroscopy for monitoring chemoresistance of cancer cells. *Micromachines* **2020**, *11*, 832. [[CrossRef](#)] [[PubMed](#)]
17. Schwan, H.P. Electrical properties of tissues and cell suspensions: Mechanisms and models. In Proceedings of the 16th Annual International Conference of the IEEE Engineering in Medicine and Biology Society, Baltimore, MD, USA, 3–6 November 1994; Volume 1, pp. A70–A71.
18. Lazanas, A.C.; Prodromidis, M.I. Electrochemical Impedance Spectroscopy—A Tutorial. *ACS Meas. Sci. Au* **2023**, *3*, 162–193. [[CrossRef](#)]
19. Teixeira, V.S.; Barth, T.; Labitzky, V.; Schumacher, U.; Krautschneider, W. Electrical Impedance Spectroscopy for Characterization of Prostate PC-3 and DU 145 Cancer Cells. *Annu. Int. Conf. IEEE Eng. Med. Biol. Soc.* **2019**, *2019*, 6485–6489. [[CrossRef](#)]
20. Schneider, D.; Tarantola, M.; Janshoff, A. Dynamics of TGF- β induced epithelial-to-mesenchymal transition monitored by electric cell-substrate impedance sensing. *Biochim. Et Biophys. Acta (BBA)-Mol. Cell Res.* **2011**, *1813*, 2099–2107. [[CrossRef](#)]
21. Zhao, Y.; Wang, K.; Chen, D.; Fan, B.; Xu, Y.; Ye, Y.; Wang, J.; Chen, J.; Huang, C. Development of microfluidic impedance cytometry enabling the quantification of specific membrane capacitance and cytoplasm conductivity from 100,000 single cells. *Biosens. Bioelectron.* **2018**, *111*, 138–143. [[CrossRef](#)]
22. Du, X.; Zhang, Z.; Zheng, X.; Zhang, H.; Dong, D.; Zhang, Z.; Liu, M.; Zhou, J. An electrochemical biosensor for the detection of epithelial–mesenchymal transition. *Nat. Commun.* **2020**, *11*, 192. [[CrossRef](#)]
23. Wei, X.; Xiong, H.; Zhou, Y.; Chen, X.; Yang, W. Tracking epithelial–mesenchymal transition in breast cancer cells based on a multiplex electrochemical immunosensor. *Biosens. Bioelectron.* **2024**, *258*, 116372. [[CrossRef](#)] [[PubMed](#)]
24. Kaighn, M.E.; Narayan, K.S.; Ohnuki, Y.; Lechner, J.F.; Jones, L.W. Establishment and characterization of a human prostatic carcinoma cell line (PC-3). *Investig. Urol.* **1979**, *17*, 16–23.
25. Stone, K.R.; Mickey, D.D.; Wunderli, H.; Mickey, G.H.; Paulson, D.F. Isolation of a human prostate carcinoma cell line (DU 145). *Int. J. Cancer* **1978**, *21*, 274–281. [[CrossRef](#)] [[PubMed](#)]
26. Horoszewicz, J.S.; Leong, S.S.; Kawinski, E.; Karr, J.P.; Rosenthal, H.; Chu, T.M.; Mirand, E.A.; Murphy, G.P. LNCaP Model of Human Prostatic Carcinoma1. *Cancer Res.* **1983**, *43*, 1809–1818.
27. Adams, T.N.; Jiang, A.Y.; Mendoza, N.S.; Ro, C.C.; Lee, D.-H.; Lee, A.P.; Flanagan, L.A. Label-free enrichment of fate-biased human neural stem and progenitor cells. *Biosens. Bioelectron.* **2020**, *152*, 111982. [[CrossRef](#)]
28. Simon, M.G.; Li, Y.; Arulmoli, J.; McDonnell, L.P.; Akil, A.; Nourse, J.L.; Lee, A.P.; Flanagan, L.A. Increasing label-free stem cell sorting capacity to reach transplantation-scale throughput. *Biomicrofluidics* **2014**, *8*, 064106. [[CrossRef](#)]
29. Hoettges, K.F.; Henslee, E.A.; Torcal Serrano, R.M.; Jabr, R.I.; Abdallat, R.G.; Beale, A.D.; Waheed, A.; Camelliti, P.; Fry, C.H.; van der Veen, D.R.; et al. Ten-Second Electrophysiology: Evaluation of the 3DEP Platform for high-speed, high-accuracy cell analysis. *Sci. Rep.* **2019**, *9*, 19153. [[CrossRef](#)] [[PubMed](#)]
30. Hübner, Y.; Hoettges, K.; Kass, G.; Ogin, S.; Hughes, M. Parallel measurements of drug actions on erythrocytes by dielectrophoresis, using a three-dimensional electrode design. In *IEE Proceedings-Nanobiotechnology*; IET: Singapore, 2005; pp. 150–154.
31. Rudzinski, J.K.; Govindasamy, N.P.; Lewis, J.D.; Jurasz, P. The role of the androgen receptor in prostate cancer-induced platelet aggregation and platelet-induced invasion. *J. Thromb. Haemost.* **2020**, *18*, 2976–2986. [[CrossRef](#)]
32. Webber, M.M.; Bello, D.; Quader, S. Immortalized and tumorigenic adult human prostatic epithelial cell lines: Characteristics and applications part I. Cell markers and immortalized nontumorigenic cell lines. *Prostate* **1996**, *29*, 386–394.

33. Cruz, M.; Sidén, Å.; Calaf, G.; Delwar, Z.; Yakisich, J. The stemness phenotype model. *Int. Sch. Res. Not.* **2012**, *2012*, 392647. [[CrossRef](#)] [[PubMed](#)]
34. Moya, L.; Walpole, C.; Rae, F.; Srinivasan, S.; Seim, I.; Lai, J.; Nicol, D.; Williams, E.D.; Clements, J.A.; Batra, J. Characterisation of cell lines derived from prostate cancer patients with localised disease. *Prostate Cancer Prostatic Dis.* **2023**, *26*, 614–624. [[CrossRef](#)] [[PubMed](#)]
35. Bagnaninchi, P.O.; Drummond, N. Real-time label-free monitoring of adipose-derived stem cell differentiation with electric cell-substrate impedance sensing. *Proc. Natl. Acad. Sci. USA* **2011**, *108*, 6462–6467. [[CrossRef](#)] [[PubMed](#)]
36. Hildebrandt, C.; Büth, H.; Cho, S.; Impidjati; Thielecke, H. Detection of the osteogenic differentiation of mesenchymal stem cells in 2D and 3D cultures by electrochemical impedance spectroscopy. *J. Biotechnol.* **2010**, *148*, 83–90. [[CrossRef](#)]
37. Song, H.; Rosano, J.M.; Wang, Y.; Garson, C.J.; Prabhakarpandian, B.; Pant, K.; Klarmann, G.J.; Perantoni, A.; Alvarez, L.M.; Lai, E. Identification of mesenchymal stem cell differentiation state using dual-micropore microfluidic impedance flow cytometry. *Anal. Methods* **2016**, *8*, 7437–7444. [[CrossRef](#)]
38. Buczek, M.E.; Miles, A.K.; Green, W.; Johnson, C.; Boocock, D.J.; Pockley, A.G.; Rees, R.C.; Hulman, G.; van Schalkwyk, G.; Parkinson, R.; et al. Cytoplasmic PML promotes TGF- β -associated epithelial–mesenchymal transition and invasion in prostate cancer. *Oncogene* **2016**, *35*, 3465–3475. [[CrossRef](#)]
39. Tirino, V.; Camerlingo, R.; Bifulco, K.; Irollo, E.; Montella, R.; Paino, F.; Sessa, G.; Carriero, M.V.; Normanno, N.; Rocco, G.; et al. TGF- β 1 exposure induces epithelial to mesenchymal transition both in CSCs and non-CSCs of the A549 cell line, leading to an increase of migration ability in the CD133+ A549 cell fraction. *Cell Death Dis.* **2013**, *4*, e620. [[CrossRef](#)]

Disclaimer/Publisher’s Note: The statements, opinions and data contained in all publications are solely those of the individual author(s) and contributor(s) and not of MDPI and/or the editor(s). MDPI and/or the editor(s) disclaim responsibility for any injury to people or property resulting from any ideas, methods, instructions or products referred to in the content.